Sensors and Actuators: A. Physical 332 (2021) 113199

Contents lists available at ScienceDirect

Sensors and Actuators: A. Physical

journal homepage: www.elsevier.com/locate/sna

3D-printed omnidirectional soft pneumatic actuators: Design, modeling and characterization

Matheus S. Xavier[a,*], Charbel D. Tawk[b], Yuen K. Yong[a], Andrew J. Fleming[a]

[a] University of Newcastle, Callaghan, NSW, Australia
[b] University of Wollongong in Dubai, Dubai Knowledge Park, Dubai, United Arab Emirates

ARTICLE INFO

Article history:
Received 4 August 2021
Received in revised form 27 September 2021
Accepted 25 October 2021
Available online 3 November 2021

Keywords:
Soft actuators
Finite element modeling
3D printing
Soft robotics
Pneumatic actuators

ABSTRACT

Soft pneumatic actuators are usually fabricated using molding and casting techniques with silicone rubbers, which requires intensive manual labor and limits repeatability and design flexibility for complex geometries. This article presents the design and direct 3D-printing of novel omnidirectional soft pneumatic actuators using stereolithography (SLA) with an elastic resin and fused deposition modeling (FDM) with a thermoplastic polyurethane (TPU). The actuator is modeled and optimized for bending performance using the finite element method along with a hyperelastic material model that is based on experimental uniaxial tensile data. The designs inspired by fast pneumatic network actuators (PneuNets) allow for multimodal actuation including bending, extension and contraction motions under positive, negative or differential pressures. The predicted results from the finite element method are compared with the experimental results for a range of actuation configurations. These novel omnidirectional actuators have significant potential in applications such as pipe inspection and biomedical devices.

1. Introduction

Soft robotics is a rapidly growing field where the robots are elastically deformable and usually follow a bio-inspired design [1,2]. Soft robots are compliant, have infinite degrees of freedom (DoF) and show high dexterity and safety [3,4]. Their ability to elastically deform and adapt their shape to external constraints and obstacles make them ideal for applications such as gripping, locomotion and medical devices, where the environment is highly dynamic and sensitive to physical interaction [5,6].

Actuation mechanisms for soft robots include tendon-driven, fluidic and smart material actuation (i.e., thermal, optical or magnetic actuation) [7,8]. Pneumatic actuation is still the dominant technology due to the light weight, fast response time and easy implementation [5,9]. A variety of soft pneumatic actuator designs has been proposed in the literature [3,10]. While single chamber actuators [11] and bellow-shaped designs have been used, the two main groups are fiber-reinforced actuators and pneumatic network actuators (PneuNets). Fiber-reinforced actuators can be used to achieve bending, extension, contraction or twisting motions with different fiber wrapping angles and anisotropic features such as differing wall thicknesses and the addition of strain limiting layers [4,12]. Fiber-reinforced actuators are also referred to as PneuFlex actuators [13,14]. PneuNets, also known as multi-chambered actuators, have been investigated in [15–18]. Slow PneuNets are discussed in [15,19], where a block of silicone rubber has embedded air chambers. In contrast, the fast PneuNets developed in [16] contains gaps between the inside walls of each chamber. The authors showed that slow PneuNets required approximately 3 times higher pressure and 8 times higher volume to fully bend compared to fast PneuNets, which also had improved speed (i.e., 25 times) and force (i.e., 1.4 times).

The complex geometries of soft actuators and the hyperelastic models used in their fabrication hinder the development of accurate mathematical models to describe their performance. Consequently, finite element modeling (FEM) has found many applications in soft robotics since it: (i) reduces cost and development time, (ii) can cope with large deformations and material nonlinearities, and (iii) can be used to predict performance and evaluate the capabilities of soft actuator designs, while improving our understanding of the stress concentration and strain distribution after pressurization [20–22].

Soft pneumatic actuators are usually fabricated with a molding process by 3D-printing molds into which silicone rubbers are cast and consolidated [23,24]. Soft actuators fabricated with silicone rubber offer durability, biocompatibility and high deformation levels at low pressures. However, the molding process is time-consuming

* Corresponding author.
E-mail address: matheus.xavier@newcastle.edu.au (M.S. Xavier).

https://doi.org/10.1016/j.sna.2021.113199
0924-4247/

and requires significant manual assembly, which can create issues with weak seams, repeatability and accuracy [25]. In addition, complex geometries often require multi-stage casts using techniques such as overmolding [26]. The final design might also require the addition of strain limiting layers or fiber reinforcements.

The monolithic fabrication approach based on directly using an additive manufacturing (AM) method is a possible solution to fabricate highly complex and optimized shapes [27]. Moving from mold fabrication to the total AM approach, the involvement of AM technologies switches from a passive role (i.e., used only to fabricate molds) to a dominant role (i.e., exclusively used for soft robots manufacturing). The use of direct additive manufacturing for soft robotic fabrication takes full advantage of the available 3D-printing technologies, such as reduced manual tasks and the ability to fabricate very complex geometries, intricate circuits, and multi-component designs in an all-in-one manufacturing setup [25,28].

2. Related work

2.1. 3D-printed soft pneumatic actuators

Due to the difficulties involved with mold-based fabrication of soft robotic actuators, a significant research investment has occurred to develop direct fabrication methods. The foremost methods are [28–30]:

1) Material extrusion: process in which material is selectively dispensed through a nozzle or orifice onto a surface, which then fuses into a solid object upon cooling. This includes FDM, which is also known as fused filament fabrication (FFF), and direct ink writing (DIW). Using DIW, bending finger pneumatic actuators were developed in [31] and multi-material soft actuators with programmable contractile, expanding and twisting motions in [32]. FDM is the most commonly used technique due to its accessibility and relatively low price [33]. The range of fabricated actuators include bending actuators [27,34–40], helical actuators [33,40,41] and vacuum-powered actuators [42,43].

2) Material jetting (i.e., Polyjet): process in which droplets of feed-stock material are selectively deposited. Modifications to a Stratasys Objet260 Connex printer were performed in [44] to fabricate actuators with solid and liquid components. A Stratasys Objet 350 Connex 3 was used to fabricate parallel bellow-shaped actuators in [45,46]. This printer was also used in [47] to incorporate embedded resistive sensors into a fast PneuNet actuator. Polyjet bellows actuators with optimized designs to improve fatigue life were fabricated in [48].

3) Vat polymerization: process in which liquid photopolymer in a vat is selectively cured by light-activated polymerization. This includes digital light processing (DLP) and stereolithography (SLA). The printing process takes place within a dense liquid bath, which reduces the requirement for support materials to print thin and hollow structures, and offers sub-micrometer resolution [49]. Micrometer scale soft pneumatic grippers were fabricated in [50,51] using DLP. In [52], micro-bellows actuators are developed for extension and bending using SLA with the SL5180 photopolymer. In [53], bidirectional actuators with a bellow structure are fabricated using a commercially available elastomeric precursor and a custom-made SLA printer.

2.2. Omnidirectional soft pneumatic actuators

Omnidirectional actuators were proposed in [58,62] and further explored in [54,55,57]. The omnidirectional actuator usually has three internal chambers (Fig. 1a,b,d,e). When all three chambers are equally pressurized, the actuator extends. In contrast, when only one or two chambers are pressurized, the actuator bends in the direction opposite to the pressurized chambers. These actuators have three DoF, which are pitch, yaw and stretch. Actuators with three DoF can also be fabricated using three parallel, externally connected actuators rotated 120 degrees about the longitudinal axis of the actuator in a design inspired by the parallel bellows actuators in pneumatic continuum robots [63,64]. Parallel actuators have been proposed in soft robotics using fiber-reinforced extending actuators [60,61] (Fig. 1h,i), off-the-shelf rubber bellows [65], 3D-printed bellows actuators [45,46] (Fig. 1g) and bellows fabricated with silicone rubber [59,66] (Fig. 1f). In contrast, omnidirectional actuators with four chambers in a multi-layer small cavity series configuration are proposed in [67] using a multi-step silicone molding process. A summary of the omnidirectional actuators in the literature is provided in Table 1.

In recent works, several 3D-printed soft pneumatic actuators have been proposed for bending (single direction and bidirectional), elongation, contraction and twisting. In contrast, omnidirectional actuators are usually fabricated using a molding process and very few works have used 3D-printing to directly fabricate these actuators. As outlined in Table 1, previous 3D-printed omnidirectional actuators have a parallel bellows structure, which essentially combines three extending actuators to generate bending. This design, however, requires multi-step fabrication and usually displays lower bending performance in comparison to molded single-structure omnidirectional actuators.

2.3. Contributions

In this article, we propose a new class of monolithic omnidirectional soft actuators, shown in Fig. 2, that utilize a fast internal pneumatic network suited to direct 3D printing in a single fabrication step. Compared to existing design concepts such as the parallel bellows actuator and fiber-reinforced actuators, the proposed method requires only one major fabrication step, and is a completely monolithic structure which does not require post-fabrication assembly or bonding. The unique mechanical properties and reduced fabrication effort are expected to be attractive in a wide variety of applications that require omnidirectional bending and extension.

The primary contributions of this article are as follows:

i. Design and single-step fabrication of novel omnidirectional soft pneumatic actuators with three and four cavities using stereolithography (SLA) with an off-the-shelf elastic resin and fused deposition modeling (FDM) with a thermoplastic polyurethane (TPU).
ii. Characterization of the hyperelastic parameters for the elastic resin used with SLA. This work reports the first application of SLA to the fabrication of omnidirectional actuators and the first application of the elastic resin from Formlabs to any type of soft bending actuator.
iii. Modeling of the bending angle and blocked force of the actuators using FEM. Using FEM, the soft actuator designs are optimized for higher bending levels at lower pressures.
iv. To demonstrate the capabilities of the actuators in achieving bending, extension and contraction motions. In addition, to demonstrate actuation performance with positive, negative or differential pressures.
v. Quantification of the soft actuators performance through experimental results and comparison to the FEM predictions for both designs and fabrication methods.

The remainder of this article is organized as follows. Section 3 presents the uniaxial tensile test results and hyperelastic material models for the elastic resin. Section 4 presents the design of the omnidirectional soft actuators and the FEM results. Section 5 describes the fabrication of the soft pneumatic actuators using SLA and FDM. In Section 6, the experimental results are presented and

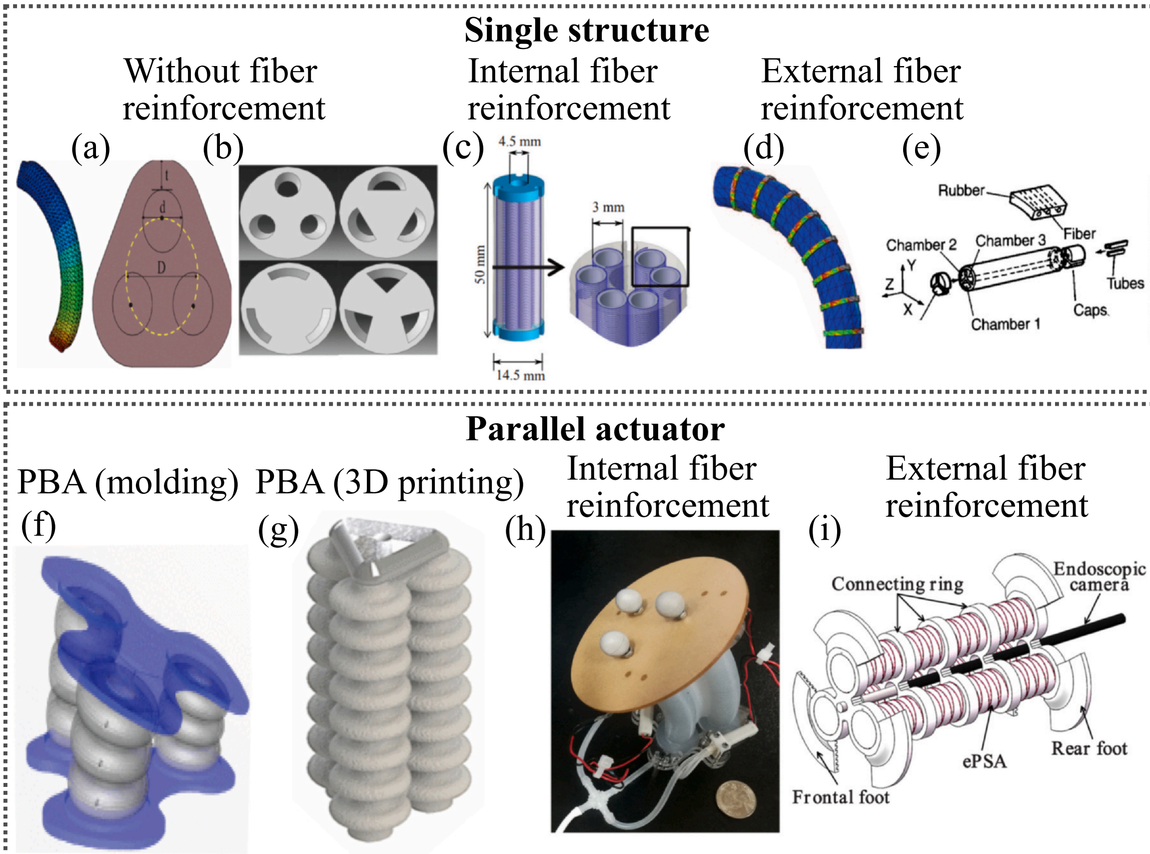

Fig. 1. Review of omnidirectional actuators in the literature. (a,b) Single structure actuators without fiber reinforcement [54,55]. (c) Single structure actuator with internal fiber reinforcement [56]. (d,e) Single structure actuator with external O-rings and fiber-reinforced rubber [57,58]. (f) PBA actuator fabricated with molding [59]. (g) PBA actuator fabricated with Polyjet [45]. (h) Parallel actuator with internal fiber reinforcement [60]. (i) Parallel actuator with external fiber reinforcement [61]. All figures are reproduced with permission.

Table 1
Review of omnidirectional soft pneumatic actuators. Bending performance results are indicated for single cavity/bellow actuation.

Design	Fabrication	Material	Bending performance	Ref.
Single structure	Molding	Elastosil M4601	180°, 1.2 N at 150 kPa	[54]
		Ecoflex30	180° at 10 kPa	[55]
		PS6600 silica gel	170° at 100 kPa, 1.5 N at 90 kPa	[67]
		Ecoflex50, external braided sheet	120° at 65 kPa	[68]
Single structure (fiber-reinforced)	Molding	Fiber-reinforced rubber	100° at 400 kPa	[58]
		Silica gel 15A, aramid fiber	81°, 4.8 N at 200 kPa	[69]
		Ecoflex30, O-rings	270° at 45 kPa	[57]
		Ecoflex50, fiber	148° at 150 kPa	[56]
Parallel bellows actuator	Molding	Silica gel	60° at 50 kPa	[59]
		Ecoflex50	80° at 48 kPa	[66]
	3D printing (Polyjet)	Veroclear and TengoBlackPlus	79°, 1.57 N at 60 kPa	[45,46]
	3D printing (SLS)	Polyamide	N/A	[70]
	Manual assembly	Off-the-shelf rubber bellows	70° at 41 kPa	[65]
Parallel actuator (fiber-reinforced)	Molding	Ecoflex50, kevlar fiber	90° at 100 kPa	[61]
		Ecoflex30, fiber	40° at 55 kPa	[60]
		DragonSkin10, fiber	100° at 172 kPa	[60]
This work	3D-printing (SLA)	Elastic resin (Formlabs)	177° at 200 kPa (3 cavity)	
			162° at 200 kPa (4 cavity)	
	3D-printing (FDM)	NinjaFlex	90° at 700 kPa (4 cavity)	

compared to the FEM predictions. Finally, Section 7 discusses the conclusions of this work.

3. Material characterization

Due to the large nonlinearities of the materials used in soft robotics, hyperelastic models are considered. Here, the materials are assumed to be isotropic and incompressible. A number of hyperelastic material models have been used in the soft robotics literature [20,71]. In this work, the Neo-Hookean and Yeoh models are considered since the material response for these models can be fairly characterized using uniaxial tensile testing [72,73].

(1) Neo-Hookean model:

$$W = C_1(I_1 - 3) = \frac{\mu}{2}(I_1 - 3) \quad (1)$$

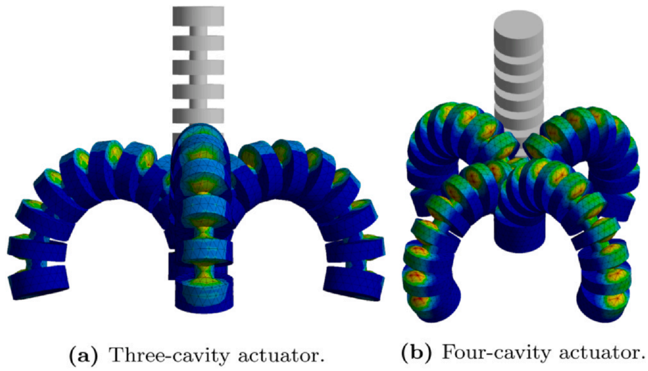

Fig. 2. Omnidirectional bending for the novel soft pneumatic actuators with (a) three and (b) four cavities.

where μ is the shear modulus, $I_1 = \lambda_1^2 + \lambda_2^2 + \lambda_3^2$ is a principal invariant and $\lambda_i = l_i/L_i$ are the stretch ratios along the principal axes given by the ratio of deformed length l_i to undeformed length L_i.

(2) Yeoh model:

$$W = C_1(I_1 - 3) + C_2(I_1 - 3)^2 + C_3(I_1 - 3)^3 \quad (2)$$

The Neo-Hookean model shows good agreement for small strains, i.e., lower than 50%. The Yeoh model is commonly used for large strain problems. In particular, the Yeoh model describes the elastic behavior with reasonable success over quite large ranges of strain and is able to predict stress-stretch behavior in different deformation modes from data gained with simple uniaxial testing. The corresponding stress-stretch equations for these models are:

(1) Neo-Hookean model:

$$\sigma = 2(\lambda^2 - \lambda^{-1})C_1 \quad (3)$$

(2) Yeoh model:

$$\sigma = 2(\lambda^2 - \lambda^{-1}) \sum_{i=1}^{n} iC_i(\lambda^2 + 2\lambda^{-1} - 3)^{i-1} \quad (4)$$

The tensile test data is force F and strain δL. These values are converted to stress σ and stretch λ using:

$$\sigma = \frac{F}{A}, \quad \lambda = \frac{L_0 + \delta L}{L_0} \quad (5)$$

where A is the initial cross-sectional area of the reduced section of the sample and L_0 is the undeformed length (Fig. 3).

NinjaFlex Midnight (NinjaTek, USA) is the TPU used in the fabrication of soft actuators with FDM. Hyperelastic constants for NinjaFlex have been characterized in a number of studies in the literature [22,36,40,41,43]. In contrast, the elastic resin (Formlabs, USA) used in this work has not been employed in soft robotics. Consequently, hyperelastic constants are not available and therefore uniaxial tensile tests are performed to obtain the material parameters required for FEM. The elastic resin has shore hardness 40A (uncured) and 50A (post-cured) and ultimate tensile strength of 1.61 MPa (uncured) and 3.23 MPa (post-cured), as provided by the supplier datasheet.

Uniaxial tensile tests were performed using Autograph AGS-X 5 kN (Shimadzu Corporation, Japan) at a rate of 50 mm/min. The elastic resin dumbbell-shaped samples were 3D printed using a Form 3 (Formlabs, USA) and follow the geometry and dimensions of the ASTM D412 standard. These samples were printed directly on the build plate with 100 μm resolution and the wash time was 20 min. For cured samples, curing was performed using Form Cure (Formlabs, USA) with curing time of 20 min and temperature of 60 °C. Initial tests revealed early failure in the region between the grip and reduced sections. Therefore, to obtain further extension during testing and better characterize the material, the final tested samples were 3D-printed with 2 mm fillets on their edges.

To determine the coefficients C_i, a nonlinear least squares optimization method is used in MATLAB to minimize the error with respect to the parameters of the model. This is achieved using the function *fit* with Eqs. (3) and (4) in the definition of *fittype*. The fitted parameters for the 3D-printed elastic resin samples with the Neo-Hookean and Yeoh models are summarized in Table 2.

4. Design and finite element modeling

4.1. Design

While bidirectional actuators can be easily achieved with two bending actuators, the design and fabrication of omnidirectional actuators is more challenging. For 3D-printed materials, the usual design for omnidirectional actuators with three or four single chambers embedded in a silicone body [57,58,74] leads to very small bending before failure of the actuator. In this work, to enhance the performance of the 3D-printed actuator, we propose a corrugated/multi-chambered design inspired by fast pneumatic network actuators. The fast PneuNet-inspired design allows for smaller change in volume (i.e., reduced radial expansion), faster actuation and higher bending at lower pressures, which are desirable features for 3D-printed soft actuators which have previously been difficult to obtain using available 3D-printing materials due to the higher stiffness than silicone rubber. In addition, these actuators can also be operated under vacuum (i.e., negative pressures) to achieve bending in the opposite direction.

The omnidirectional actuators proposed here are modeled in Autodesk Inventor (Autodesk Inc.) using the parameters shown in Fig. 4. In particular, two types of actuators are proposed: the first includes a series of chambers in four cavities (Fig. 4c), while the second has a series of chambers in three cavities (Fig. 4d). Both of these designs allow for omnidirectional bending and extension with appropriate selection of pressurized cavities, as shown in Fig. 5. While both actuators can be used to achieve omnidirectional bending (particularly when combining varying pressures at different chambers), a larger number of cavities can be used to improve the precision of the manipulation of the actuator within their respective workspace. The selection of actuator design is, therefore, application and performance dependent. Further, the selection of the actuator design should also be based on the number of independent pneumatic sources or simultaneous controllers/valves used in the pneumatic system.

4.2. Finite element modeling

The soft actuators are modeled in ANSYS Mechanical (ANSYS Inc.) using Static Structural Analysis. The following settings are used in the analysis: mesh size of 3 mm with nonlinear mechanical physics preference and tetrahedral elements, auto time stepping with minimum time step of 3 ms and maximum time step of 50 ms and large deflections enabled. The boundary conditions are as follows: (i) Fixed Support at the bottom wall to mimic the behavior of the clamping mechanism, and (ii) a pressure applied normally to the internal wall cavities.

To improve the bending performance of the omnidirectional actuators and minimize the required input pressure, the key parameters in the designs are evaluated. As the actuators are modular with respect to the number of chambers, the length is not a key parameter and is fixed to 110 mm, which corresponds to 11 modules or groups of chambers. The diameter of the actuators is also fixed at 24 mm. The critical parameters are identified to be the midsection radius r_m, top wall thickness t_t, side wall thickness t_s and internal wall thickness t_i, whose values for both designs are as follows:

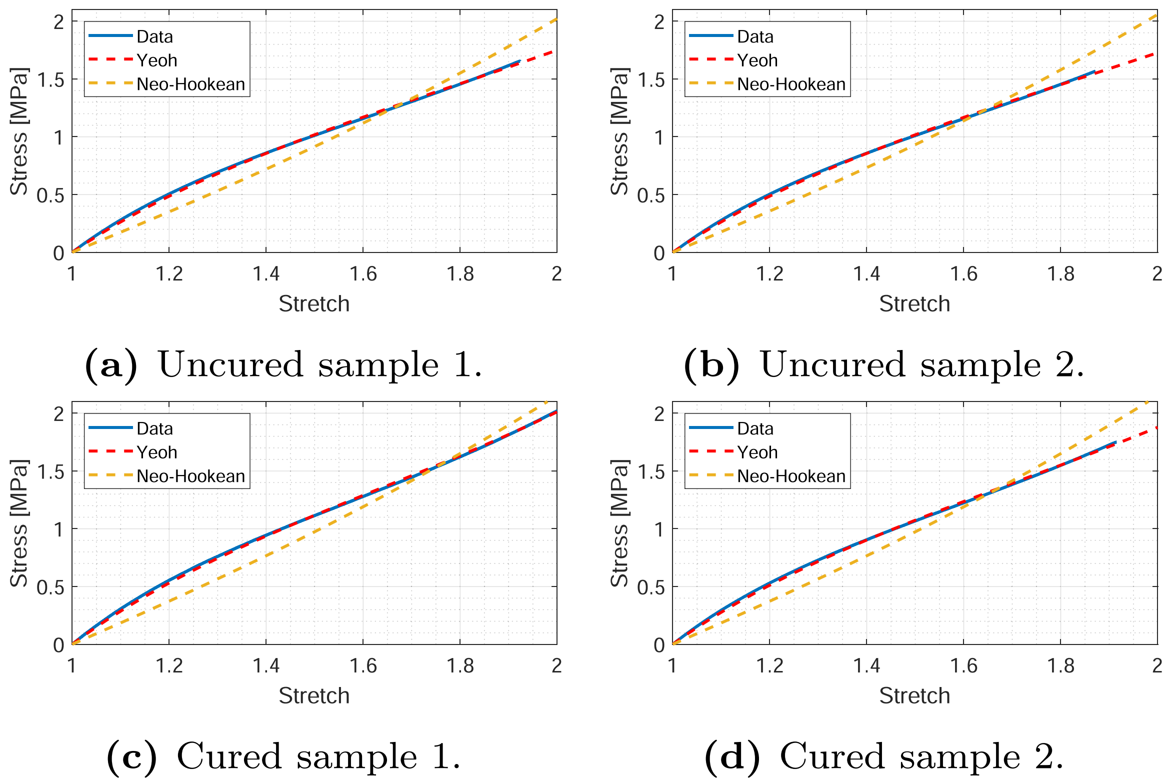

(a) Uncured sample 1. (b) Uncured sample 2.

(c) Cured sample 1. (d) Cured sample 2.

Fig. 3. Uniaxial tensile test data and fitted models for elastic resin dog-bone test samples. The top row displays the curve fitting approach for two uncured samples and the bottom row displays the approach for two cured samples.

Table 2
Hyperelastic material model constants for the elastic resin.

Sample	Model	Parameters (MPa)
Uncured 1	Neo-Hookean	$C_1 = 0.2889$
	Yeoh	$C_1 = 0.4802$, $C_2 = 0$, $C_3 = 0.001626$
Uncured 2	Neo-Hookean	$C_1 = 0.2931$
	Yeoh	$C_1 = 0.4804$, $C_2 = 0$, $C_3 = 0.001076$
Cured 1	Neo-Hookean	$C_1 = 0.3074$
	Yeoh	$C_1 = 0.5243$, $C_2 = 0$, $C_3 = 0.004186$
Cured 2	Neo-Hookean	$C_1 = 0.3072$
	Yeoh	$C_1 = 0.5056$, $C_2 = 0$, $C_3 = 0.002562$

1. midsection radius r_m: 3 mm, 4.5 mm and 6 mm.
2. top wall thickness t_t: 1 mm, 1.5 mm and 2.5 mm.
3. side wall thickness t_s: 1 mm, 1.5 mm and 2 mm.
4. internal wall thickness t_i: 1 mm, 1.5 mm and 2 mm.

The Yeoh model demonstrated better agreement with the experimental results, hence the averaged constants from the two uncured samples are used in the FEM simulations presented in this work. The FEM results for single cavity actuation of the four-cavity actuator are shown in Fig. 6. Results for the three-cavity actuator follow similar trends and are not included for the sake of brevity.

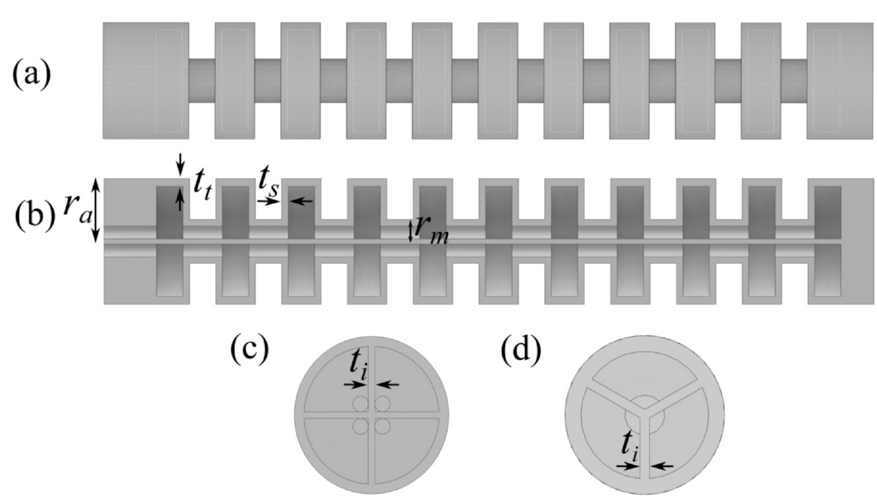

Fig. 4. Omnidirectional actuator designs and geometrical parameters: (a) side view, (b) side cross-section view, (c) radial cross-section view of the four-cavity actuator and (d) radial cross-section view of the three-cavity actuator. The geometrical parameters are: actuator radius r_a, midsection radius r_m, side wall thickness t_s, top wall thickness t_t and internal wall thickness t_i. The actuator length is fixed at 110 mm and the radius r_a at 12 mm.

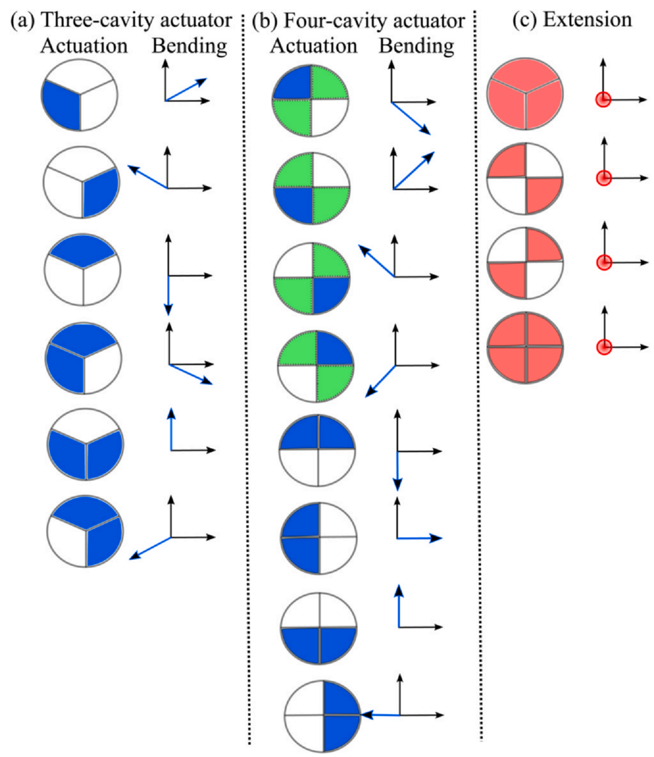

Fig. 5. Actuation modes for omnidirectional actuator designs: the colored cavity indicates actuation with positive pressure and the respective arrow indicates the bending direction. (a) Three-cavity actuator: bending can be achieved by actuation of single or double cavities. (b) Four-cavity actuator: bending can be achieved by actuation of single, double or triple cavities. Note that actuation of triple cavities (indicated in both blue and green) lead to the same bending direction as single cavity actuation (indicated in blue only). (c) Extension can be achieved with pressurization of all three cavities of the three-cavity actuator or at least two opposing cavities for the four-cavity actuator. (For interpretation of the references to color in this figure legend, the reader is referred to the web version of this article.)

Low values of the mid section radius result in strong ballooning of the chambers, while large values increase the overall stiffness of the actuator, which both result in reduced bending. Reduced top wall thickness leads to improved bending performance. However, it also results in large ballooning of the chamber walls, which potentially reduces the fatigue life of the actuator. For the 1 mm top wall thickness, the simulations failed to converge after approximately 160 degrees for the elastic resin material.

The side and internal wall thickness are the most important parameters that define the performance of the actuators, with smaller values leading to higher bending angles. To ensure air tightness of the 3D-printed samples and improve fatigue performance, while minimizing the pressure input, the final actuator design uses the following parameters: mid section radius of 4.5 mm, top wall thickness of 1.5 mm, side wall thickness of 1 mm and internal wall thickness of 1 mm.

The performance of the four-cavity omnidirectional actuator for single, double, triple and quadruple cavity actuation is displayed in Fig. 7. For this actuator, in comparison to the pressurization of one cavity (Fig. 7a), the actuation of two side cavities provides larger bending at lower pressure values (Fig. 7b), while triple cavity actuation decreases the bending angle for equivalent pressure values (Fig. 7c). Further, the actuation of all four cavities leads to extension of the actuator (Fig. 7d).

The fast pneumatic network design of the proposed omnidirectional actuators allows for pressurization with both positive and negative pressures. The results for actuation with negative pressures are shown in Fig. 8. Negative pressures allow for motion in the opposite direction in comparison to the positive pressures in Fig. 7. Further, they also allow for a small level of contraction of the actuator. It is important to note that actuation with negative pressures provides a fail-safe feature, i.e., the performance of the actuators is

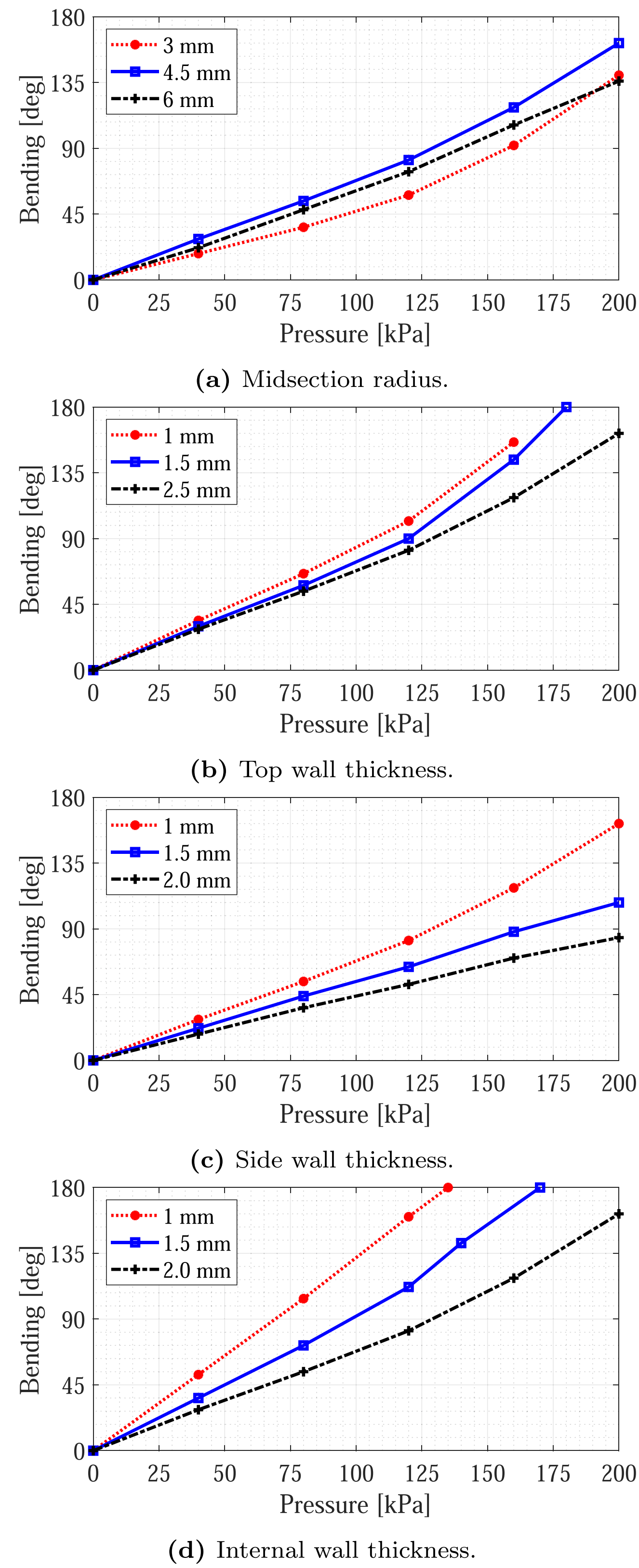

Fig. 6. Design optimization for the parameters of omnidirectional actuators with four cavities using FEM.

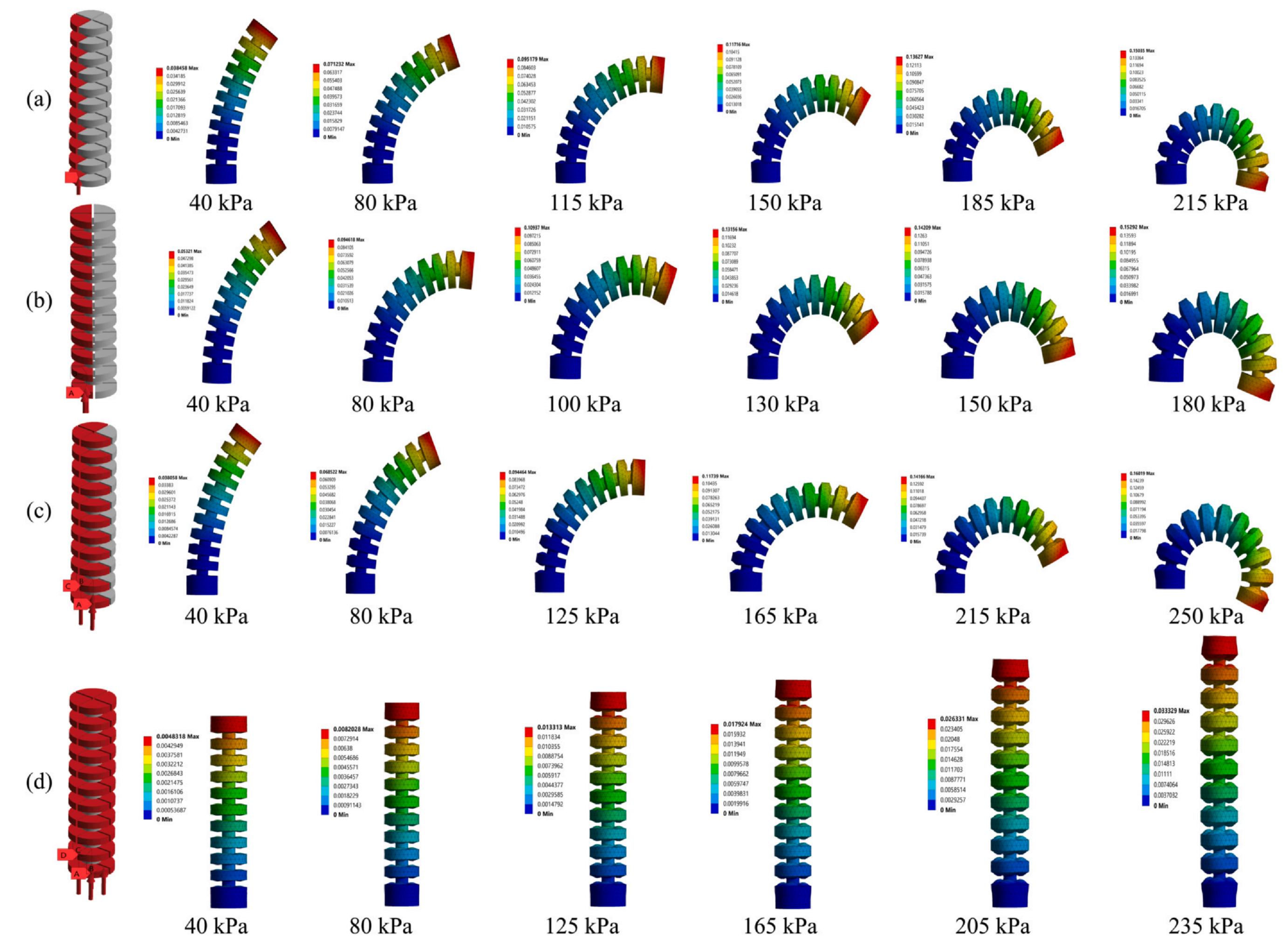

Fig. 7. Finite element simulation of the four-cavity actuator for a range of positive pressure levels: (a) single cavity actuation, (b) double cavity actuation, (c) triple cavity actuation and (d) quadruple cavity actuation. The actuated cavities are shown in red (labels can be ignored) and the legends show the total deformation in meters.

not affected by minor leaks or structural damage, which improves robustness, durability and lifetime.

The performance of the omnidirectional actuators can be further improved using a combination of positive and negative pressure, as illustrated in Fig. 9. The results show that the achievable workspace of the soft actuator increases by using differential pressure values, i.e., higher bending angles can be achieved with reduced positive pressure values.

4.3. Blocked force

In addition to the displacement, the blocked force is an important performance metric for soft actuators. The blocked force is the force generated by the tip of the soft actuator and represents the ability of the actuator to convert pressure to force.

For the blocked force simulations in ANSYS, a fixed support was assigned to the proximal end of the actuator, which therefore acts as a cantilever beam. Force measurements are obtained using a displacement support at the tip of the actuator, which allows the distal end of the actuator to slide friction-free across the displacement support modeling the load cell [21], as shown in Fig. 10. This displacement support resists the bending deformation of the soft actuator during pressurization, consequently the actuator bends backwards in an arch and slides over the displacement support.

Blocked force measurements are summarized in Table 3 for three and four-cavity actuators. Overall, NinjaFlex actuators are stiffer and allow for higher pressure input, which results in larger blocked forces. These forces are within the range reported for previous soft pneumatic actuators [17,45,54,67,75].

5. Fabrication

5.1. Fabrication with SLA

The omnidirectional actuators are printed using elastic resin (Formlabs, USA) and a Form 3 printer (Formlabs, USA). The printing parameters are set up in the software PreForm (Formlabs, USA), as shown in Table 4.

The parts are oriented with the bottom layer parallel to the build platform. A high support density is used to avoid print failures due to the softness of the material. Internal supports are disabled to reduce the chance of rupture during pressurization. Additional support parameters are selected to minimize the volume of elastic resin used during 3D-printing. The printing time for a single actuator with the SLA method is approximately 6 h and 40 min.

Following the 3D printing process, the actuators are washed in two plastic buckets with isopropyl alcohol (IPA) for ten minutes each and the support structures are removed. A longer washing time may cause the material to absorb solvent. To remove the uncured resin in the actuator chambers, a syringe filled with IPA is used to flush out the cavities and negative pressure is applied to the chambers using an empty syringe to remove the remaining IPA and uncured resin.

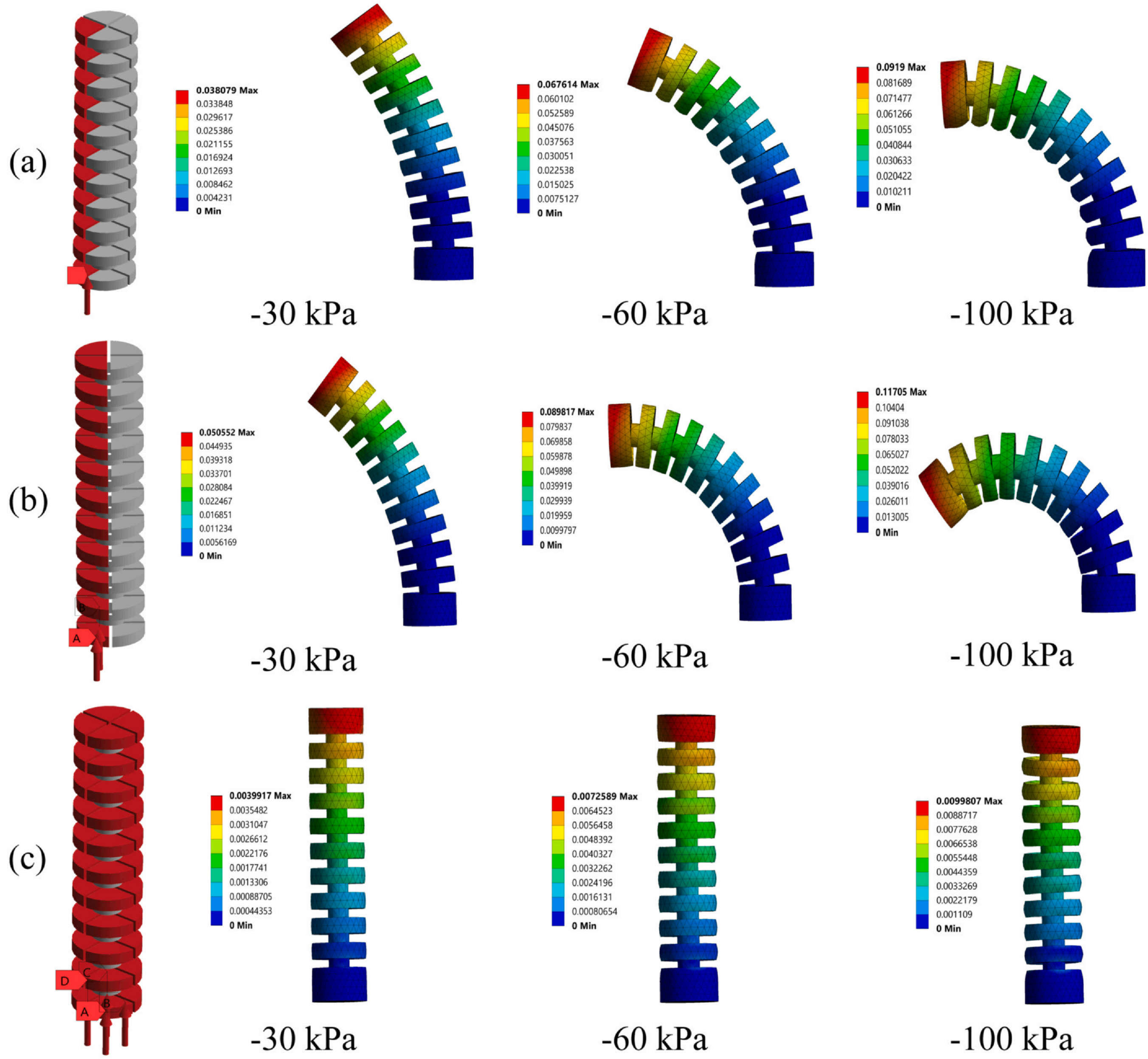

Fig. 8. Finite element simulation of the four-cavity actuator for a range of negative pressure levels: (a) single cavity actuation, (b) double cavity actuation and (c) quadruple cavity actuation. The actuated cavities are shown in red (labels can be ignored) and the legends show the total deformation in meters.

5.2. Fabrication with FDM

The omnidirectional actuators fabricated from elastic resin with stereolithography are compared to actuators fabricated from soft TPU with FDM. In the latter, the 3D models of the omnidirectional actuators are sliced using a commercial slicing software (Simplify3D LLC, OH, USA). The optimized printing parameters used to achieve airtight actuators are listed in Table 5. The actuators are fabricated using a Flashforge Inventor (Flashforge Corporation, USA) and the soft TPU NinjaFlex Midnight (NinjaTek, USA) with a diameter of 1.75 mm. Post-processing is performed by removing the support structures. The printing time of a single actuator with the FDM method is approximately 29 h and 20 min.

The first layer height and width are adjusted to ensure the first layer of the actuators adheres to the heated bed. The first layer settings are adjusted to obtain an even and complete first layer as this layer dictates the overall quality of the actuators [43]. To avoid any printed plastic residuals between the different layers, the retraction settings are set to moderate values since high retraction values lead to under-extrusion. The printing speed chosen ensures continuous and consistent printed lines and layers. High speeds are avoided as they lead to under-extrusion with soft materials. In addition, the speed of the external perimeter was reduced to obtain higher quality exteriors.

The printing temperature is chosen to ensure that the printed layers are fused but avoid over-melting the filament, which can lead to the formation of air bubbles and under-extrusion. The heated bed temperature is chosen to ensure that the first layer sticks to the bed throughout the printing process and the actuators can be easily removed when the printing process is finished by avoiding any bonding to the heated bed. The cooling speed is set to its maximum value to quickly solidify the printed layers, which avoids sagging due to the overhangs in the structure of the actuators. The infill is set to its maximum value to obtain solid walls and the perimeter overlap is

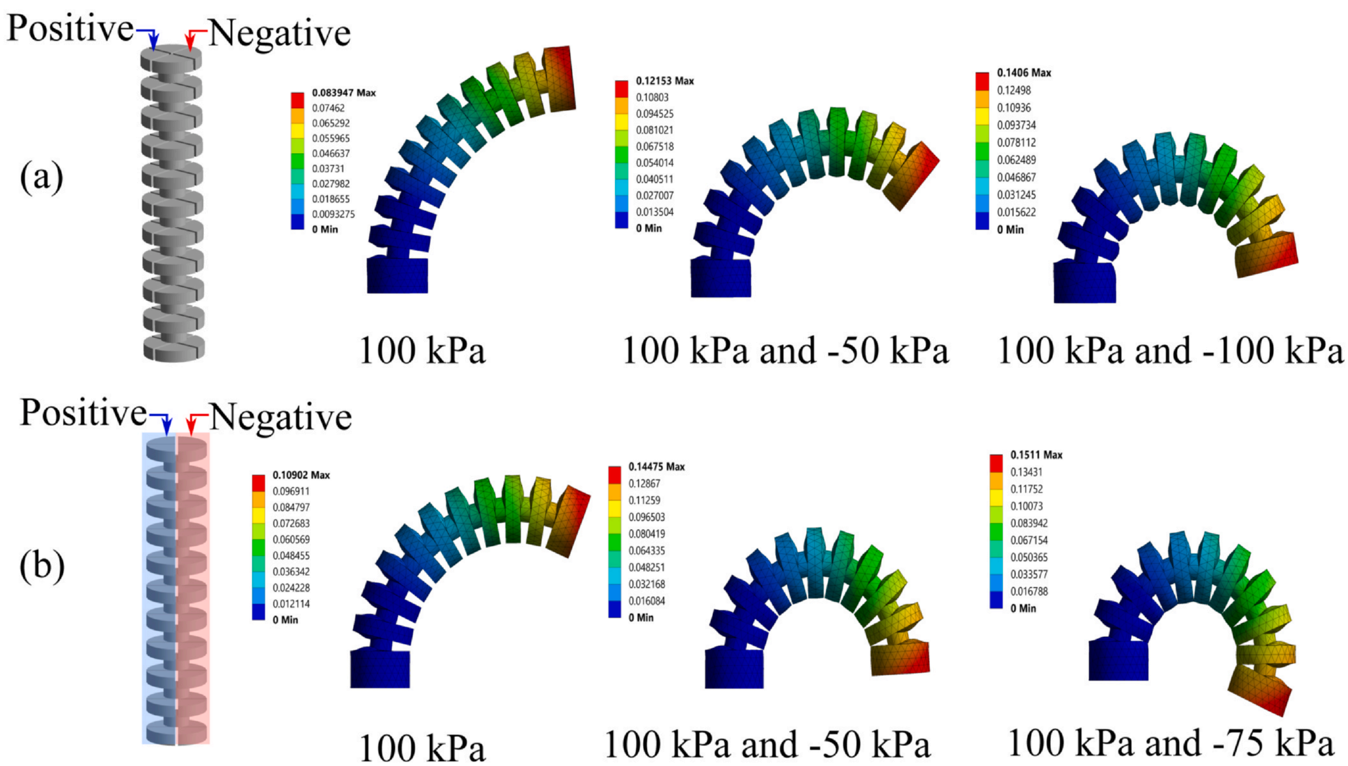

Fig. 9. Finite element simulation of the four-cavity actuator for differential pressures, i.e., a combination of positive and negative pressures. (a) Single cavity actuated with positive pressure and opposing single cavity actuated with negative pressure. (b) Two cavities actuated with positive pressure and opposing two cavities actuated with negative pressure. The legends show the total deformation in meters.

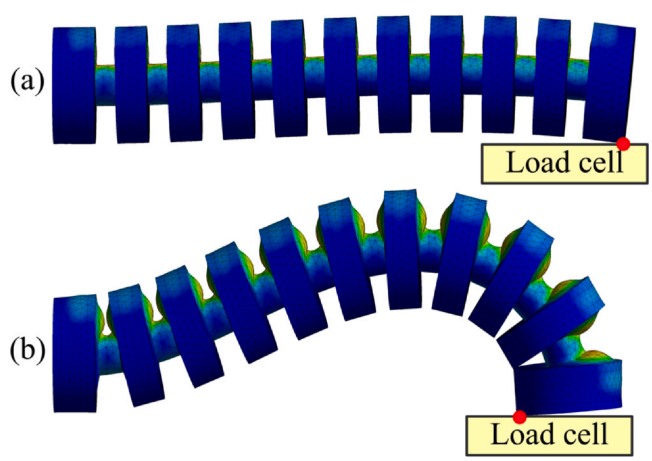

Fig. 10. Finite element simulation for blocked force measurements of a three-cavity actuator with single cavity actuation and pressures of (a) 10 kPa and (b) 200 kPa. The actuator is fixed at one end using a fixed support, while a displacement support at the actuator tip models the load cell. The force sensor probe is indicated by the red circle.

Table 3
Blocked force measurements in ANSYS. The column "Cavities" indicates the number of actuated cavities with the respective pressure.

Actuator type	Material	Cavities	Pressure (kPa)	Blocked force (N)
3 Cavities	Elastic resin	1	200	0.2196
3 Cavities	Elastic resin	2	200	0.1884
3 Cavities	NinjaFlex	1	700	0.5517
3 Cavities	NinjaFlex	2	700	0.5035
4 Cavities	Elastic resin	1	200	0.2750
4 Cavities	Elastic resin	2	200	0.4969
4 Cavities	NinjaFlex	1	700	0.8123
4 Cavities	NinjaFlex	2	700	1.1524

Table 4
3D-printing and post-processing parameters for SLA with elastic resin.

Parameter	Value	Unit
Printing resolution	100	μm
Resin tank temperature	31	°C
Support density	1	
Touchpoint size of support	0.7	mm
Internal supports	Disabled	
Height above raft	3	mm
Raft thickness	2.5	mm
Flat spacing	4	mm
Slope multiplier	1	
Wash time	20	min
Curing time	20	min
Curing temperature	60	°C

chosen to ensure that the infill and perimeters are fused with no air gaps.

The "Avoid Crossing Outline" option is enabled to ensure that the nozzle does not cross the perimeters throughout the printing process, which avoids the generation of plastic residuals that in turn lead to air gaps between the layers of the 3D-printed actuators. The extrusion multiplier is increased to avoid under-extrusion throughout the printing process since the TPU is soft and to account for any inconsistencies in the diameter of the TPU filament.

6. Characterization

6.1. Characterization and comparison to FE

A custom-made 60 mL syringe pump [76] is used to pressurize the omnidirectional actuator with air. A pressure sensor (SEN0257, DFRobot) connected to an Arduino Due is inserted between the syringe and the actuator. PLX-DAQ is used to store the real-time pressure measurements. The actuator is clamped horizontally, a

Table 5
3D-printing parameters for NinjaFlex using FDM.

Parameter	Value	Unit
Resolution settings		
Primary layer height	0.1	mm
First layer height	0.09	mm
First layer width	0.125	mm
Extrusion width	0.4	mm
Retraction settings		
Retraction length	4	mm
Retraction speed	40	mm/s
Speed settings		
Default printing speed	10	mm/s
Outline printing speed	8	mm/s
Solid infill speed	8	mm/s
First layer speed	8	mm/s
Temperature settings		
Printing temperature	230	°C
Heat bed temperature	32	°C
Cooling settings		
Fan speed	100	%
Infill settings		
Infill percentage	100	
Infill/parameter overlap	30	
Thin walls		
Allowed perimeter overlap	15	
External thin wall type	Perimeters only	
Internal thin wall type	Single extrusion fill	
Movements behavior		
Avoid crossing outline	Enabled	
Additional settings		
Extrusion multiplier	1.15	
Wipe nozzle	Disabled	
Support material	Enabled	

video camera with 60 frames per second is used to capture the motion of the actuator and the software Kinovea is used to measure the bending angles.

Upon fabrication, it is clear that gravity plays an important role in the actuator bending performance. To account for that, the finite element simulations are performed in two steps. In the first step, the model is simulated only for gravity. Then, once steady-state is reached, the pressure value is increased in time steps of 3 ms. The actuator is fixed at its base and simulated horizontally to account for the gravity effect. The 3D printed dumbbell-shaped samples used for material characterization have a mass of 0.6 g and the volume is obtained from Autodesk Inventor as 5.02 cm^3, consequently the density used for the elastic resin simulations is 1.2 g/cm^3.

Experimental and FEM results for the four-cavity actuator fabricated with SLA are compared in Fig. 11a for two load conditions: gravity only and 180 degrees bending. A similar comparison for a three-cavity actuator is shown in Fig. 11b. The results for an omnidirectional actuator fabricated with NinjaFlex are presented in Fig. 11c. In the latter, FEM results are obtained using a density of 1.19 g/cm^3 and a five parameter Mooney-Rivlin hyperelastic model with $C_{10} = -0.233$, $C_{01} = 2.562$, $C_{20} = 0.116$, $C_{11} = -0.561$, $C_{02} = 0.900$ MPa [22,43].

Experimental results and FEM predictions for the bending angle versus pressure are shown in Fig. 12 for the elastic resin omnidirectional actuators with three and four cavities. The FEM results underestimate the bending due to gravity loading only and initial pressure levels and tend to overestimate the bending for pressure levels above 100 kPa. A similar trend is observed for the NinjaFlex omnidirectional actuator, as shown in Fig. 13. This may indicate the need to consider compressibility, viscoelasticity and stress softening in the constitutive model of the elastic resin and NinjaFlex.

6.2. Discussion

As expected, for single cavity actuation, the actuator with three cavities (Fig. 12c) outperforms the actuator with four cavities (Fig. 12a). However, actuation of two cavities for the latter significantly improves bending performance, as shown in Fig. 12b. In contrast, double cavity actuation of the three-cavity actuator only slightly improves bending performance (Fig. 12d).

The disparities between the experimental and FEM results are likely to be associated with the uniaxial tensile tests used to characterize the elastic resin and NinjaFlex samples, and the fabrication tolerance and nonuniform walls of the 3D-printed actuators in comparison to the 3D models. The differences could also be associated with the printing resolution and the requirement for support structures during printing, where removal of the latter may cause a small level of warping. For the elastic resin actuators, uncured resin in the internal cavities of the actuator and a small amount of residue support attached to the walls also affect the bending performance. Further, to reduce the number of mesh elements and facilitate convergence, the air channels in the lumen between the chambers have not been included in the simulation.

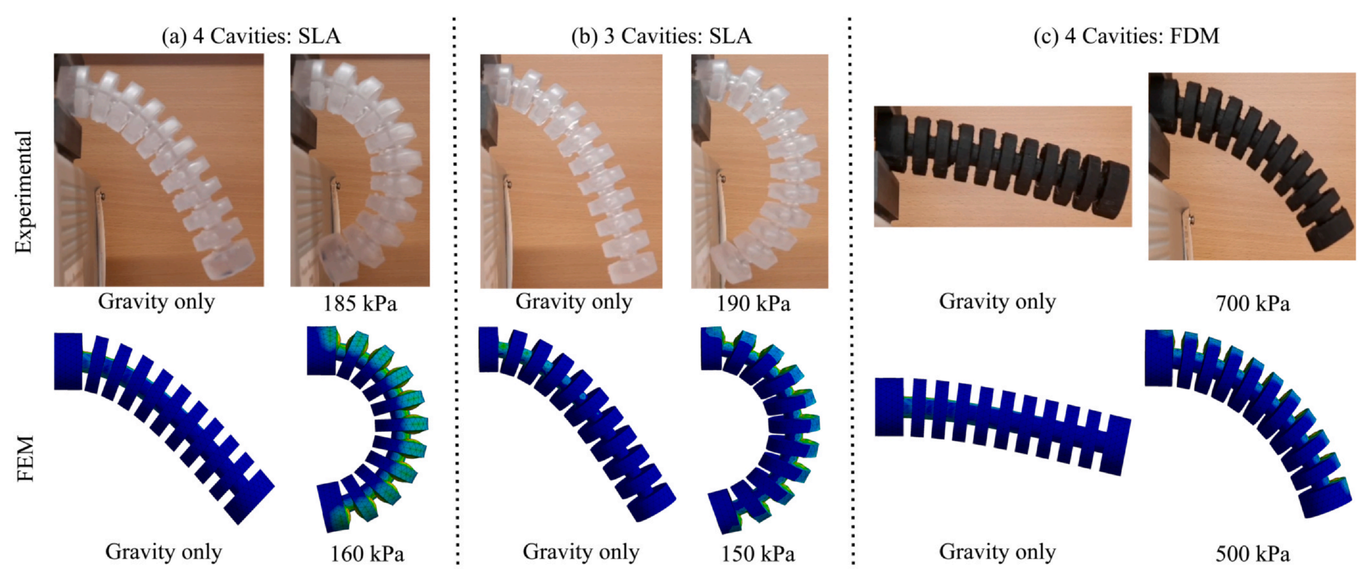

Fig. 11. Comparison between experimental and FEM results for gravity load only and selected pressure values. (a) Four-cavity SLA actuator where the top two cavities are actuated. (b) Three-cavity SLA actuator where the top cavity is actuated. (c) Four-cavity FDM actuator where the top cavity is actuated.

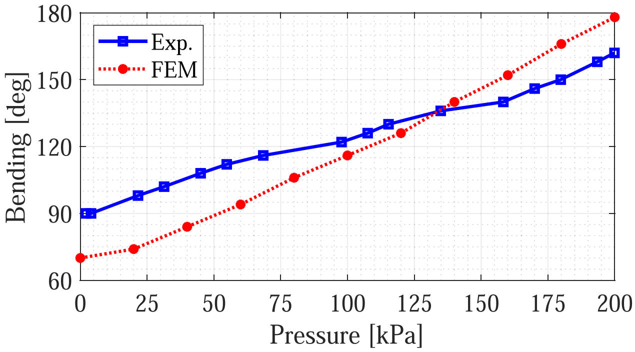

(a) Four-cavity actuator with single cavity actuation.

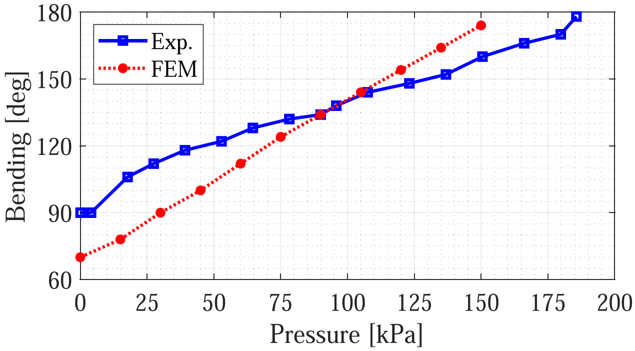

(b) Four-cavity actuator with double cavity actuation.

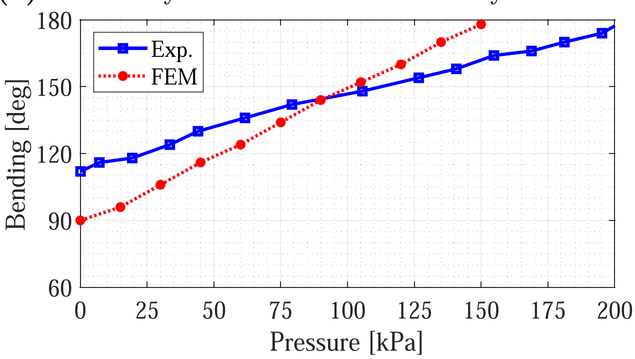

(c) Three-cavity actuator with single cavity actuation.

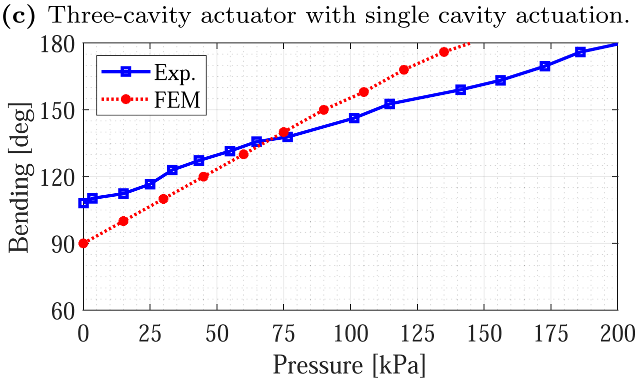

(d) Three-cavity actuator with double cavity actuation.

Fig. 12. Comparison of experimental and FEM results for the bending angle of three- and four-cavity actuators fabricated with SLA.

The main advantage of the FEM approach is that it allows the optimization of the soft actuator performance by varying geometrical parameters or material models to obtain the desired performance, which reduces cost and development time since the fabrication of soft fluidic actuators is very time-consuming.

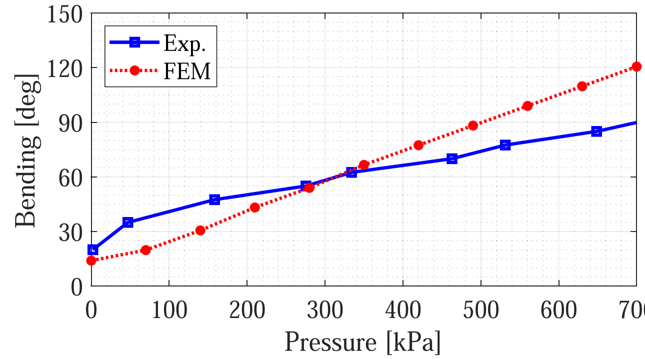

Fig. 13. Comparison of experimental and FEM results for the bending angle of a four-cavity actuator fabricated with FDM.

FDM is the most popular method for direct 3D-printing of soft actuators due to the low cost and minimal post-processing. However, soft actuators fabricated with FDM usually have a rougher surface finish and limited resolution. Moreover, FDM printed materials are usually harder and require very high pressure levels to reach deformation levels that are comparable to actuators fabricated from silicone rubbers or photocurable resins and elastomers. This is clearly noted in Fig. 13, which shows that the bending angle is below 120 degrees at a pressure of 700 kPa, whereas the elastic resin actuators can achieve the same bending level at 100 kPa or less (Figs. 7 and 12).

The SLA method employed in this work offers improved printing resolution, surface quality and printing speed in comparison to FDM. The softer nature of the elastic resin allows for significant bending at pressure levels below 200 kPa, which facilitates fabricating air-tight actuators. In addition, lower pressures are better suited for biomedical devices and require lower cost pneumatic sources. However, disadvantages include the high cost of the elastic resin, tacky surfaces, the need to remove internal uncured resin and the possibility of post-curing warping. Furthermore, the elastic resin offers lower fatigue durability since it can only elongate to 100% (uncured) or 160% (post-cured) in comparison to elongation of up to 660% for NinjaFlex.

7. Conclusions and future work

This work describes a new class of omnidirectional soft actuators, which are optimized for direct 3D printing using either stereolithograhy with an elastic resin, or fused deposition modeling with a thermoplastic polyurethane. The actuator design uses a series of chambers in three- or four-cavity configurations to achieve bending, extension and contraction. Uniaxial material testing was performed to identify the hyperelastic model parameters for the elastic resin. These models were then utilized to perform finite element simulations and optimize the geometry of the proposed actuators. The experiments show good correlation between the simulated predictions and experimental results. Bending angles of up to 180 degrees were characterized with pressures up to 200 kPa for the elastic resin actuators.

The proposed actuators and fabrication methods have significant advantages for applications such as worm and snake-like robots, especially in biomedical and pipe inspection devices. Future work includes the miniaturization of these actuators for applications in minimally invasive surgical devices.

CRediT authorship contribution statement

Matheus S. Xavier: Conceptualization, Methodology, Software, Investigation, Formal analysis, Visualization, Writing – original draft, Writing – review & editing, Project administration. **Charbel D. Tawk:** Conceptualization, Software, Investigation, Formal analysis, Writing – original draft, Writing – review & editing. **Yuen K. Yong:** Writing – review & editing, Supervision, Funding acquisition. **Andrew J. Fleming:** Writing – review & editing, Supervision, Funding acquisition.

Declaration of Competing Interest

The authors declare that they have no known competing financial interests or personal relationships that could have appeared to influence the work reported in this paper.

References

[1] D. Rus, M. Tolley, Design, fabrication and control of soft robots, Nature 521 (7553) (2015) 467–475, https://doi.org/10.1038/nature14543
[2] S. Kim, C. Laschi, B. Trimmer, Soft robotics: a bioinspired evolution in robotics, Trends Biotechnol. 31 (5) (2013) 287–294, https://doi.org/10.1016/j.tibtech.2013.03.002
[3] L. Hines, K. Petersen, G. Lum, M. Sitti, Soft actuators for small-scale robotics, Adv. Mater. 29 (13). 10.1002/adma.201603483.
[4] P. Polygerinos, Z. Wang, J. Overvelde, K. Galloway, R. Wood, K. Bertoldi, C. Walsh, Modeling of soft fiber-reinforced bending actuators, IEEE Trans. Robot. 31 (3) (2015) 778–789, https://doi.org/10.1109/TRO.2015.2428504
[5] C. Tawk, G. Alici, A review of 3d-printable soft pneumatic actuators and sensors: research challenges and opportunities, Adv. Intell. Syst. (2021) 2000223.
[6] J. Gul, M. Sajid, M. Rehman, G. Siddiqui, I. Shah, K.-H. Kim, J.-W. Lee, K. Choi, 3d printing for soft robotics-a review, Sci. Technol. Adv. Mater. 19 (1) (2018) 243–262, https://doi.org/10.1080/14686996.2018.1431862
[7] Y. Yang, Y. Wu, C. Li, X. Yang, W. Chen, Flexible actuators for soft robotics, Adv. Intell. Syst. 2 (1) (2020) 1900077, https://doi.org/10.1002/aisy.201900077
[8] N. El-Atab, R.B. Mishra, F. Al-Modaf, L. Joharji, A.A. Alsharif, H. Alamoudi, M. Diaz, N. Qaiser, M.M. Hussain, Soft actuators for soft robotic applications: a review, Adv. Intell. Syst. 2 (10) (2020) 2000128, https://doi.org/10.1002/aisy.202000128
[9] G.M. Whitesides, Soft robotics, Angew. Chem. Int. Ed. 57 (16) (2018) 4258–4273.
[10] B. Gorissen, D. Reynaerts, S. Konishi, K. Yoshida, J.-W. Kim, M.De Volder, Elastic inflatable actuators for soft robotic applications, Adv. Mater. 29 (43). 10.1002/adma.201604977.
[11] S. Konishi, F. Kawai, P. Cusin, Thin flexible end-effector using pneumatic balloon actuator, Sens. Actuator A Phys. 89 (1–2) (2001) 28–35, https://doi.org/10.1016/S0924-4247(00)00533-1
[12] K. Galloway, P. Polygerinos, C. Walsh, R. Wood, Mechanically programmable bend radius for fiber-reinforced soft actuators, in: Proceedings of International Conference on Advanced Robotics, 2013. 10.1109/ICAR.2013.6766586.
[13] M. Memarian, R. Gorbet, D. Kulić, Control of soft pneumatic finger-like actuators for affective motion generation, in: Proceedings of the IEEE/RSJ International Conference on Intelligent Robots and Systems, IEEE, 2015, 1691–1697.
[14] R. Deimel, O. Brock, A compliant hand based on a novel pneumatic actuator, in: Proceedings of IEEE International Conference on Robotics and Automation, IEEE, 2013, 2047–2053.
[15] R. Shepherd, F. Ilievski, W. Choi, S. Morin, A. Stokes, A. Mazzeo, X. Chen, M. Wang, G. Whitesides, Multigait soft robot, Proc. Natl. Acad. Sci. USA 108 (51) (2011) 20400–20403, https://doi.org/10.1073/pnas.1116564108
[16] B. Mosadegh, P. Polygerinos, C. Keplinger, S. Wennstedt, R. Shepherd, U. Gupta, J. Shim, K. Bertoldi, C. Walsh, G. Whitesides, Pneumatic networks for soft robotics that actuate rapidly, Adv. Funct. Mater. 24 (15) (2014) 2163–2170, https://doi.org/10.1002/adfm.201303288
[17] P. Polygerinos, S. Lyne, Z. Wang, L. Nicolini, B. Mosadegh, G. Whitesides, C. Walsh, Towards a soft pneumatic glove for hand rehabilitation, in: Proceedings of the IEEE/RSJ International Conference on Intelligent Robots and Systems, 2013, pp. 1512–1517. 10.1109/IROS.2013.6696549.
[18] Y. Hwang, O. Paydar, R. Candler, Pneumatic microfinger with balloon fins for linear motion using 3d printed molds, Sens. Actuator A Phys. 234 (2015) 65–71, https://doi.org/10.1016/j.sna.2015.08.008
[19] Y. Sun, Y. Song, J. Paik, Characterization of silicone rubber based soft pneumatic actuators, in: Proceedings of the IEEE/RSJ International Conference on Intelligent Robots and Systems, 2013, pp. 4446–4453. 10.1109/IROS.2013.6696995.
[20] M.S. Xavier, A.J. Fleming, Y.K. Yong, Finite element modeling of soft fluidic actuators: overview and recent developments, Adv. Intell. Syst. 3 (2) (2021) 2000187.
[21] P. Moseley, J.M. Florez, H.A. Sonar, G. Agarwal, W. Curtin, J. Paik, Modeling, design, and development of soft pneumatic actuators with finite element method, Adv. Eng. Mater. 18 (6) (2016) 978–988.
[22] C. Tawk, G. Alici, Finite element modeling in the design process of 3d printed pneumatic soft actuators and sensors, Robotics 9 (3) (2020) 52.
[23] A. Marchese, R. Katzschmann, D. Rus, A recipe for soft fluidic elastomer robots, Soft Robot. 2 (1) (2015) 7–25, https://doi.org/10.1089/soro.2014.0022
[24] F. Schmitt, O. Piccin, L. Barbé, B. Bayle, Soft robots manufacturing: a review, Front. Robot. AI 5 (2018) 84.
[25] S. Walker, O. Yirmibeşoğlu, U. Daalkhaijav, Y. Mengüç, Additive manufacturing of soft robots, Robotic Systems and Autonomous Platforms, Elsevier, 2019, pp. 335–359.
[26] T. Hainsworth, L. Smith, S. Alexander, R. MacCurdy, A fabrication free, 3d printed, multi-material, self-sensing soft actuator, IEEE Robot. Autom. Lett. 5 (3) (2020) 4118–4125.
[27] H.M. Anver, R. Mutlu, G. Alici, 3d printing of a thin-wall soft and monolithic gripper using fused filament fabrication, in: IEEE International Conference on Advanced Intelligent Mechatronics (AIM), IEEE, 2017, pp. 442–447.
[28] G. Stano, G. Percoco, Additive manufacturing aimed to soft robots fabrication: a review, Extrem. Mech. Lett. (2020) 101079.
[29] T. Wallin, J. Pikul, R. Shepherd, 3d printing of soft robotic systems, Nat. Rev. Mater. 3 (6) (2018) 84–100, https://doi.org/10.1038/s41578-018-0002-2
[30] A. Zolfagharian, M.P. Mahmud, S. Gharaie, M. Bodaghi, A.Z. Kouzani, A. Kaynak, 3d/4d-printed bending-type soft pneumatic actuators: fabrication, modelling, and control, Virtual Phys. Prototyp. 15 (4) (2020) 373–402.
[31] J. Plott, A. Shih, The extrusion-based additive manufacturing of moisture-cured silicone elastomer with minimal void for pneumatic actuators, Addit. Manuf. 17 (2017) 1–14.
[32] M. Schaffner, J.A. Faber, L. Pianegonda, P.A. Rühs, F. Coulter, A.R. Studart, 3d printing of robotic soft actuators with programmable bioinspired architectures, Nat. Commun. 9 (1) (2018) 1–9.
[33] W. Hu, G. Alici, Bioinspired three-dimensional-printed helical soft pneumatic actuators and their characterization, Soft Robot. 7 (3) (2020) 267–282.
[34] H.K. Yap, H.Y. Ng, C.-H. Yeow, High-force soft printable pneumatics for soft robotic applications, Soft Robot. 3 (3) (2016) 144–158.
[35] W. Irawan, A.S. Ritonga, A. Prastowo, et al., Design and fabrication in the loop of soft pneumatic actuators using fused deposition modelling, Sens. Actuator A Phys. 298 (2019) 111556.
[36] K.G. Demir, Z. Zhang, J. Yang, G.X. Gu, Computational and experimental design exploration of 3d-printed soft pneumatic actuators, Adv. Intell. Syst. 2 (7) (2020) 2000013.
[37] G. Stano, L. Arleo, G. Percoco, Additive manufacturing for soft robotics: design and fabrication of airtight, monolithic bending pneunets with embedded air connectors, Micromachines 11 (5) (2020) 485.
[38] Q. Ji, X. Zhang, M. Chen, X.V. Wang, L. Wang, L. Feng, Design and closed loop control of a 3d printed soft actuator, in: IEEE International Conference on Automation Science and Engineering (CASE), IEEE, 2020, pp. 842–848.
[39] M.A. Saleh, M. Soliman, M.A. Mousa, M. Elsamanty, A.G. Radwan, Design and implementation of variable inclined air pillow soft pneumatic actuator suitable for bioimpedance applications, Sens. Actuator A Phys. 314 (2020) 112272.
[40] B.A.W. Keong, R.Y.C. Hua, A novel fold-based design approach toward printable soft robotics using flexible 3d printing materials, Adv. Mater. Technol. 3 (2) (2018) 1700172.
[41] L. Rosalia, B.W.-K. Ang, R.C.-H. Yeow, Geometry-based customization of bending modalities for 3d-printed soft pneumatic actuators, IEEE Robot. Autom. Lett. 3 (4) (2018) 3489–3496.
[42] C. Tawk, M. in het Panhuis, G.M. Spinks, G. Alici, Bioinspired 3d printable soft vacuum actuators for locomotion robots, grippers and artificial muscles, Soft Robot. 5 (6) (2018) 685–694.
[43] C. Tawk, G.M. Spinks, M. in het Panhuis, G. Alici, 3d printable linear soft vacuum actuators: their modeling, performance quantification and application in soft robotic systems, IEEE ASME Trans. Mechatron. 24 (5) (2019) 2118–2129.
[44] R. MacCurdy, R. Katzschmann, Y. Kim, D. Rus, Printable hydraulics: a method for fabricating robots by 3d co-printing solids and liquids, in: IEEE International Conference on Robotics and Automation (ICRA), IEEE, 2016, pp. 3878–3885.
[45] T. Kalisky, Y. Wang, B. Shih, D. Drotman, S. Jadhav, E. Aronoff-Spencer, M. Tolley, Differential pressure control of 3d printed soft fluidic actuators, in: Proceedings of IEEE/RSJ IEEE International Conference on Intelligent Robots and Systems, 2017, pp. 6207–6213. 10.1109/IROS.2017.8206523.
[46] D. Drotman, M. Ishida, S. Jadhav, M. Tolley, Application-driven design of soft, 3-d printed, pneumatic actuators with bellows, IEEE ASME Trans. Mechatron. 24 (1) (2019) 78–87, https://doi.org/10.1109/TMECH.2018.2879299
[47] B. Shih, C. Christianson, K. Gillespie, S. Lee, J. Mayeda, Z. Huo, M.T. Tolley, Design considerations for 3d printed, soft, multimaterial resistive sensors for soft robotics, Front. Robot. AI 6 (2019) 30.
[48] G. Dämmer, S. Gablenz, A. Hildebrandt, Z. Major, Polyjet-printed bellows actuators: design, structural optimization, and experimental investigation, Front. Robot. AI 6 (2019) 34.
[49] D.K. Patel, A.H. Sakhaei, M. Layani, B. Zhang, Q. Ge, S. Magdassi, Highly stretchable and uv curable elastomers for digital light processing based 3d printing, Adv. Mater. 29 (15) (2017) 1606000.
[50] Y.-F. Zhang, C.J.-X. Ng, Z. Chen, W. Zhang, S. Panjwani, K. Kowsari, H.Y. Yang, Q. Ge, Miniature pneumatic actuators for soft robots by high-resolution multi-material 3d printing, Adv. Mater. Technol. 4 (10) (2019) 1900427.
[51] L. Ge, L. Dong, D. Wang, Q. Ge, G. Gu, A digital light processing 3d printer for fast and high-precision fabrication of soft pneumatic actuators, Sens. Actuator A Phys. 273 (2018) 285–292.
[52] H.-W. Kang, I. Lee, D.-W. Cho, Development of a micro-bellows actuator using micro-stereolithography technology, 4-9 SPEC. ISS. Microelectron. Eng. 83 (2006) 1201–1204, https://doi.org/10.1016/j.mee.2006.01.228
[53] B.N. Peele, T.J. Wallin, H. Zhao, R.F. Shepherd, 3d printing antagonistic systems of artificial muscle using projection stereolithography, Bioinspir. Biomim. 10 (5) (2015) 055003.

[54] R. Xie, M. Su, Y. Zhang, Y. Guan, 3d-psa: a 3d pneumatic soft actuator with extending and omnidirectional bending motion, in: Proceedings of IEEE International Conference on Robotics and Biomimetics, IEEE, 2018, pp. 618–623.
[55] Y. Elsayed, C. Lekakou, T. Geng, C.M. Saaj, Design optimisation of soft silicone pneumatic actuators using finite element analysis, in: Proceedings of IEEE/ASME International Conference on Advanced Intelligent Mechatronics, IEEE, 2014, pp. 44–49.
[56] H. Abidi, G. Gerboni, M. Brancadoro, J. Fras, A. Diodato, M. Cianchetti, H. Wurdemann, K. Althoefer, A. Menciassi, Highly dexterous 2-module soft robot for intra-organ navigation in minimally invasive surgery, Int. J. Med. Robot. Comput. Assist. Surg. 14 (1) (2018) e1875.
[57] J. Yan, H. Dong, X. Zhang, J. Zhao, A three-chambed soft actuator module with omnidirectional bending motion, in: Proceedings of IEEE International Conference on Real-time Computing and Robotics, IEEE, 2016, pp. 505–510.
[58] K. Suzumori, S. Iikura, H. Tanaka, Flexible microactuator for miniature robots, in: Proceedings of IEEE Micro Electro Mechanical Systems, 1991, pp. 204–209.
[59] J. Zhang, H. Wei, Y. Shan, P. Li, Y. Zhao, L. Qi, H. Yu, Modeling and experimental study of a novel multi-dof parallel soft robot, IEEE Access 8 (2020) 62932–62942.
[60] Y. Qin, Z. Wan, Y. Sun, E. Skorina, M. Luo, C. Onal, Design, fabrication and experimental analysis of a 3-d soft robotic snake, in: Proceedings of IEEE International Conference on Soft Robotics, 2018, pp. 77–82. 10.1109/ROBOSOFT.2018.8404900.
[61] Z. Zhang, X. Wang, S. Wang, D. Meng, B. Liang, Design and modeling of a parallel-pipe-crawling pneumatic soft robot, IEEE Access 7 (2019) 134301–134317.
[62] K. Suzumori, S. Iikura, H. Tanaka, Development of flexible microactuator and its applications to robotic mechanisms, in: Proceedings of IEEE International Conference on Robotics and Automation, 2, 1991, pp. 1622–1627.
[63] A. De Greef, P. Lambert, A. Delchambre, Towards flexible medical instruments: review of flexible fluidic actuators, Precis. Eng. 33 (4) (2009) 311–321, https://doi.org/10.1016/j.precisioneng.2008.10.004
[64] D. O′Brien, D. Lane, 3d force control system design for a hydraulic parallel bellows continuum actuator, in: Proceedings of IEEE International Conference on Robotics and Automation, 3, 2001, pp. 2375–2380.
[65] N. Garbin, L. Wang, J. Chandler, K. Obstein, N. Simaan, P. Valdastri, A disposable continuum endoscope using piston-driven parallel bellow actuator, in: Proceedings of International Symposium on Medical Robotics, 2018-January, 2018, pp. 1–6. 10.1109/ISMR.2018.8333287.
[66] Z. Xue, Q. Wu, F. Gao, Design and modeling of omni-directional bending pneumatic flexible arm, in: Proceedings of International Conference on Advanced Robotics and Mechatronics, IEEE, 2018, pp. 835–839.
[67] W. Huang, Z. Xu, J. Xiao, W. Hu, H. Huang, F. Zhou, Multimodal soft robot for complex environments using bionic omnidirectional bending actuator, IEEE Access 8 (2020) 193827–193844.
[68] M. Cianchetti, T. Ranzani, G. Gerboni, I. De Falco, C. Laschi, A. Menciassi, Stiff-flop surgical manipulator: mechanical design and experimental characterization of the single module, in: Proceedings of IEEE/RSJ IEEE International Conference on Intelligent Robots and Systems, 2013, pp. 3576–3581. 10.1109/IROS.2013.6696866.
[69] J. Zhang, J. Zhou, Z.K. Cheng, S. Yuan, Fabrication, mechanical modeling, and experiments of a 3d-motion soft actuator for flexible sensing, IEEE Access 8 (2020) 159100–159109.
[70] V. Falkenhahn, A. Hildebrandt, R. Neumann, O. Sawodny, Dynamic control of the bionic handling assistant, IEEE ASME Trans. Mechatron. 22 (1) (2016) 6–17.
[71] L. Marechal, P. Balland, L. Lindenroth, F. Petrou, C. Kontovounisios, F. Bello, Toward a common framework and database of materials for soft robotics, Soft Robot. 8 (3) (2021) 284–297.
[72] B.B.S. AidyAli, M. Hosseini, A review of constitutive models for rubber-like materials, Am. J. Eng. Appl. Sci. 3 (1) (2010) 232–239.
[73] A.N. Gent, Engineering with Rubber, Hanser, 2012. 10.3139/9783446428713.fm.
[74] Y. Elsayed, A. Vincensi, C. Lekakou, T. Geng, C. Saaj, T. Ranzani, M. Cianchetti, A. Menciassi, Finite element analysis and design optimization of a pneumatically actuating silicone module for robotic surgery applications, Soft Robot 1 (4) (2014) 255–262.
[75] W. Hu, R. Mutlu, W. Li, G. Alici, A structural optimisation method for a soft pneumatic actuator, Robotics 7 (2) (2018) 24.
[76] M.S. Xavier, A.J. Fleming, Y.K. Yong, Image-guided locomotion of a pneumatic-driven peristaltic soft robot, Proceedings of IEEE International Conference on Robotics and Biomimetics, IEEE, 2019, pp. 2269–2274.

Matheus S. Xavier received his B.S. degree in Science and Technology and his B.Eng. degree in Control and Automation Engineering from the Federal University of ABC, Brazil, in 2016 and 2017, respectively. He is currently a Ph.D. student at the Precision Mechatronics Laboratory, The University of Newcastle, Australia. His research interests include soft robotics, mechatronics design, biomedical devices, and nonlinear control.

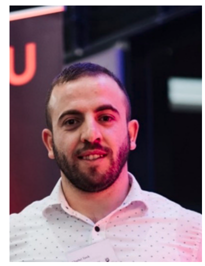

Charbel D. Tawk received his B.E. in Mechanical Engineering with high distinction from the Lebanese American University (LAU) in 2016 and his Ph.D. in Soft Robotics from The University of Wollongong, Australia, and the ARC Centre of Excellence for Electromaterials Science (ACEs), in 2019. He is currently an Assistant Professor of Mechanical Engineering at the University of Wollongong in Dubai. He was a Postdoctoral Research Fellow from 2019 to 2020 with the University of Wollongong, Australia, where he worked on soft prosthetic hands with sensing capabilities, soft wearable devices, and soft dexterous grippers. His research interests include soft and smart 3D printed actuators and sensors, soft and smart prosthetic hands, wearable soft robotic devices, and soft human-machine interfaces.

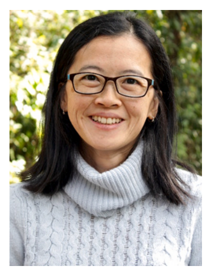

Yuen Kuan Yong received the Bachelor of Engineering degree in Mechatronics Engineering and the Ph.D. degree in mechanical engineering from The University of Adelaide, Australia, in 2001 and 2007, respectively. She was an Australian Research Council DECRA Fellow from 2013 to 2017. She is currently an associate professor with the School of Electrical Engineering and Computing, The University of Newcastle, Australia. Her research interests include miniature robotics, nanopositioning systems, and design and control of novel micro-cantilevers. A/Prof Yong is the recipient of the University of Newcastle Vice-Chancellor's Award for Research Excellence in 2014, and the Vice-Chancellor's Award for Research Supervision Excellence in 2017. She is an associate editor for the IEEE/ASME Transactions of Mechatronics.

Andrew J. Fleming graduated from The University of Newcastle, Australia, with a Bachelor of Electrical Engineering in 2000 and Ph.D. in 2004. Prof Fleming is the Director of the Precision Mechatronics Lab at The University of Newcastle, Australia. His research interests include soft medical devices, nano-positioning and scanning probe microscopy. Prof Fleming's research awards include the ATSE Baterham Medal in 2016, the IEEE Control Systems Society Outstanding Paper Award in 2007, and The University of Newcastle Researcher of the Year Award in 2007. He is the co-author of three books and more than 180 Journal and Conference articles. Prof Fleming is the inventor of several patent applications, and in 2012 he received the Newcastle Innovation Rising Star Award for Excellence in Industrial Engagement.